PRAMANA — journal of physics
© Indian Academy of Sciences
Vol. 81, No. 1
July 2013
pp. 127–141

Vibrational resonance in the Morse oscillator

K ABIRAMI[1], S RAJASEKAR[1,*] and M A F SANJUAN[2]

[1]School of Physics, Bharathidasan University, Tiruchirapalli 620 024, India
[2]Nonlinear Dynamics, Chaos and Complex Systems Group, Departamento de Física, Universidad Rey Juan Carlos, Tulipán s/n, 28933 Móstoles, Madrid, Spain
*Corresponding author. E-mail: rajasekar@cnld.bdu.ac.in; nk.abirami@gmail.com; miguel.sanjuan@urjc.es

MS received 21 June 2012; revised 8 February 2013; accepted 26 February 2013

Abstract. The occurrence of vibrational resonance is investigated in both classical and quantum mechanical Morse oscillators driven by a biharmonic force. The biharmonic force consists of two forces of widely different frequencies ω and Ω with $\Omega \gg \omega$. In the damped and biharmonically driven classical Morse oscillator, by applying a theoretical approach, an analytical expression is obtained for the response amplitude at the low-frequency ω. Conditions are identified on the parameters for the occurrence of resonance. The system shows only one resonance and moreover at resonance the response amplitude is $1/d\omega$ where d is the coefficient of linear damping. When the amplitude of the high-frequency force is varied after resonance the response amplitude does not decay to zero but approaches a nonzero limiting value. It is observed that vibrational resonance occurs when the sinusoidal force is replaced by a square-wave force. The occurrence of resonance and antiresonance of transition probability of quantum mechanical Morse oscillator is also reported in the presence of the biharmonic external field.

Keywords. Morse oscillator; biharmonic force; vibrational resonance.

PACS Nos 46.40.Ff; 05.45.−a

1. Introduction

Amplification and detection of weak signals are important in many branches of science. During the past two decades, a great deal of attention has been focussed on signal processing in nonlinear systems. There are few interesting ways of enhancing the response of a nonlinear system to a weak signal. In stochastic resonance, an optimum weak noise amplifies the response of a nonlinear system using the bistability of the system [1,2]. In another approach the noise is replaced by a high-frequency periodic signal. That is, the system is essentially driven by two periodic signals of widely different frequencies, say, ω and Ω with $\Omega \gg \omega$. When the amplitude of the high-frequency external force

DOI: 10.1007/s12043-013-0546-z; ***e*Publication: 8 June 2013**

is varied, the oscillation amplitude of the system at the low-frequency ω exhibits resonance. This high-frequency force-induced resonance is termed as vibrational resonance [3–5]. One-way or unidirectional coupling can also improve the performance of coupled systems [6–8]. The same phenomenon can also be observed when besides a noise or a high-frequency signal, a chaotic signal is used to perturb the system [9,10].

The study of vibrational resonance in the presence of a biharmonic force has received considerable attention in recent years after the seminal paper by Landa and McClintock [3]. The occurrence of vibrational resonance has been analysed in systems with monostable [11], bistable [3–5], spatially periodic states [12], excitable systems [13,14], coupled oscillators [15] and small-world networks [14,16,17]. Experimental evidence of vibrational resonance in vertical cavity laser system [18–20] and in an electronic circuit [21] has also been reported. Frequency-resonance-enhanced vibrational [22] and undamped signal propagation in one-way coupled oscillators [23] and maps [24] assisted by biharmonic force are found to occur as well.

It is important to investigate the vibrational resonance in different kinds of systems and bring out its various features and the influence of characteristics of the potential of the system on it. In this connection we point out that (i) one or more resonances in monostable systems [11], (ii) a sequence of resonance peaks in a spatially periodic potential system [12], (iii) additional resonances due to asymmetry in the potential [25], periodic and quasiperiodic occurrence of resonance peaks in time-delayed feedback systems [26–29] and large amplitude of vibrational resonance at the dynamic bifurcation point [30] have been reported.

Motivated by some of the previous results, in the present paper we report our investigation on the vibrational resonance in the Morse oscillator. The potential of the Morse oscillator is

$$V(x) = \frac{1}{2}\beta e^{-x}(e^{-x} - 2), \tag{1}$$

where β is a constant parameter representing the dissociation energy. Figure 1 depicts the form of the potential for a few values of β. The potential is nonpolynomial and $V(x) \to \infty$ as $x \to -\infty$ while it becomes zero when $x \to \infty$. It has one local minimum

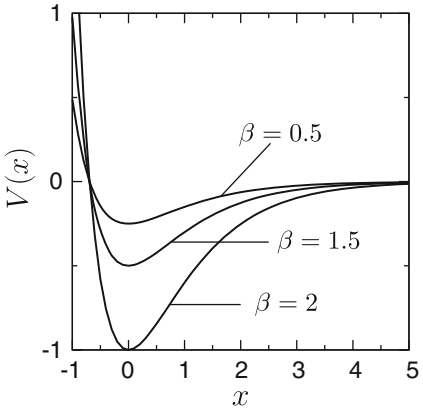

Figure 1. The shape of the Morse potential for three values of β.

at $x = 0$ and the depth of the potential is $\beta/2$. The Morse oscillator was introduced as a useful model for the interatomic potential and fitting the vibrational spectra of diatomic molecules. It was also used to describe the photodissociation of molecules, multiphoton excitation of the diatomic molecules in a dense medium or in a gaseous cell under high pressure and pumping of a local model of a polyatomic molecule by an infrared laser [31–34]. The existence and bifurcations of periodic orbits have been studied in detail in [35,36].

The equation of motion of the damped and biharmonically-driven classical Morse oscillator is given by

$$\ddot{x} + d\dot{x} + \beta e^{-x}(1 - e^{-x}) = f \cos \omega t + g \cos \Omega t, \quad \Omega \gg \omega. \tag{2}$$

Because of the difference in time-scales of the two periodic forces, the motion of system (2) contains both a slow component $X(t)$ with period $T = 2\pi/\omega$ and a fast varying component $\psi(t,\ \tau = \Omega t)$ with period $2\pi/\Omega$. That is, we assumed that $x(t) = X(t) + \psi(t, \tau)$. When the amplitude g or frequency Ω is varied, the response of system (2) at the frequency ω can exhibit resonance at a particular value of the control parameter g or Ω. To analyse this resonance phenomenon and the influence of the shape of the potential on the resonance we obtained an equation of motion for the slow variable by applying a perturbation theory. From the solution of the linearized version of the equation of motion about its equilibrium point, we found the analytical expression for the response amplitude Q which is the ratio of the amplitude of oscillation of the output of the system at the frequency ω and the amplitude f of the input signal. From the expression of Q, we extracted various features of vibrational resonance in the Morse oscillator. Particularly, we determined the value of g at which resonance occurs, the maximum value of Q at resonance and the limiting value of Q. We confirmed all the theoretical predictions through numerical simulation. The theoretical treatment used for the analysis of the vibrational resonance with the periodic force $f \cos \omega t + g \cos \Omega t$ can be applied for other types of biharmonic forces. In particular, we illustrated this for a square-wave form of low-frequency and high-frequency forces. Next, we considered the quantum mechanical Morse oscillator subjected to the biharmonic external field. Applying a perturbation theory we obtained an analytical expression for the first-order transition probability P_{fi} for a transition from an ith quantum state to an fth quantum state in time T caused by the applied external field. We analysed the influence of high-frequency field on P_{fi} and showed the occurrence of resonance and antiresonance.

2. Classical Morse oscillator

In this section the classical Morse oscillator described by the equation of motion (2) is considered and the occurrence of vibrational resonance is analysed.

2.1 *Theoretical approach*

To find an approximate solution of eq. (2), we used the method of separation of variables by assuming $x = X(t) + \psi(t,\ \tau = \Omega t)$, where X and ψ are slow and fast variables

respectively. Substituting $x = X + \psi$ in eq. (2) and adding and subtracting the terms $\beta\langle e^{-\psi}\rangle e^{-x}$ and $\beta\langle e^{-2\psi}\rangle e^{-2x}$ where $\langle u\rangle = (1/2\pi)\int_0^{2\pi} u\, d\tau$, $\tau = \Omega t$ we obtain

$$\ddot{X} + d\dot{X} + \beta e^{-X}(\langle e^{-\psi}\rangle - \langle e^{-2\psi}\rangle e^{-X}) = f\cos\omega t, \tag{3}$$

$$\ddot{\psi} + d\dot{\psi} + \beta e^{-X}(e^{-\psi} - \langle e^{-\psi}\rangle) - \beta e^{-2X}(e^{-2\psi} - \langle e^{-2\psi}\rangle) = g\cos\Omega t. \tag{4}$$

As ψ is a rapidly changing variable with fast time τ we approximated eq. (4) as $\ddot{\psi} = g\cos\Omega t$. The solution of this equation is $\psi = \mu\cos\Omega t$ where $\mu = g/\Omega^2$. This solution gives

$$\langle e^{-\psi}\rangle = \frac{1}{2}\int_0^{2\pi} e^{\mu\cos\tau}\, d\tau = I_0(\mu), \tag{5a}$$

$$\langle e^{-2\psi}\rangle = I_0(2\mu), \tag{5b}$$

where $I_0(z)$ is the zeroth-order modified Bessel function [37]. Now, eq. (3) becomes

$$\ddot{X} + d\dot{X} + \beta e^{-X}(I_0(\mu) - I_0(2\mu)e^{-X}) = f\cos\omega t. \tag{6}$$

Equation (6) can be treated as the equation of motion of a particle experiencing the external periodic force $f\cos\omega t$ and linear friction force in the effective potential

$$V_{\text{eff}} = \frac{1}{2}\beta e^{-X}[I_0(2\mu)e^{-X} - 2I_0(\mu)]. \tag{7}$$

In addition to the parameter β, the effective potential depends on the parameters g and Ω. The dependence of V_{eff} on g and Ω is in the form of a zeroth-order modified Bessel function.

Figure 2a depicts the variation of $I_0(\mu)$ and $I_0(2\mu)$ with g for $\Omega = 10$. As g increases from zero, the values of $I_0(\mu)$ and $I_0(2\mu)$ increase from the value 1. $I_0(2\mu)$ increases more rapidly than $I_0(\mu)$ with g. Figure 2b shows the change in the shape of the effective potential with g. The location of the minimum of the potential $V_{\text{eff}}(X)$ or the X-component of the equilibrium point of the system (6) in the absence of periodic driving force is given by

$$X^* = -\ln\left(\frac{I_0(\mu)}{I_0(2\mu)}\right). \tag{8}$$

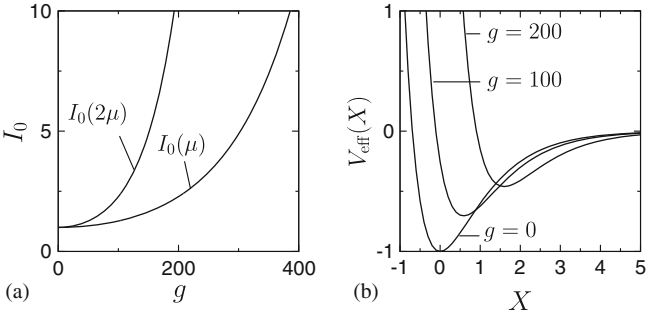

Figure 2. (**a**) Dependence of zeroth-order modified Bessel function with the control parameter g when $\Omega = 10$ and $\mu = g/\Omega^2$. (**b**) Plot of the effective potential V_{eff} given by eq. (7) for three values of g with $\beta = 2$ and $\Omega = 10$.

As $I_0(2\mu) > I_0(\mu)$, X^* is always greater than 0 and it moves away from the origin as g increases. Consequently, the depth $\Delta V_{\text{eff}} = |V_{\text{eff}}(X^*)| = \beta I_0^2(\mu)/2I_0(2\mu)$ decreases with increase in g and the potential V_{eff} becomes more and more flat. Later, we pointed out an important consequence of this on the response amplitude Q.

A slow oscillation takes place about X^*. Therefore, for convenience, a change of variable $Y = X - X^*$ is introduced so that slow oscillation occurs around $Y^* = 0$. In terms of Y, eq. (6) becomes

$$\ddot{Y} + d\dot{Y} + \omega_{\text{r}}^2 \text{e}^{-Y}(1 - \text{e}^{-Y}) = f\cos\omega t, \tag{9a}$$

where

$$\omega_{\text{r}}^2 = \beta \frac{I_0^2(\mu)}{I_0(2\mu)}. \tag{9b}$$

For $|f| \ll 1$ it is reasonable to assume that the amplitude of Y is small so that series expansions for e^{-Y} and e^{-2Y} can be written and nonlinear terms in Y can be neglected. This results in the linear equation

$$\ddot{Y} + d\dot{Y} + \omega_{\text{r}}^2 Y = f\cos\omega t. \tag{10}$$

ω_{r} is the resonant frequency of oscillation of the slow motion. In the long time limit, the solution of eq. (10) is $Y = Qf\cos(\omega t + \phi)$ where

$$Q = \frac{1}{\sqrt{S}}, \qquad S = (\omega_{\text{r}}^2 - \omega^2)^2 + d^2\omega^2, \tag{11a}$$

and

$$\phi = \tan^{-1}\left(\frac{d\omega}{\omega^2 - \omega_{\text{r}}^2}\right), \tag{11b}$$

where Q is the response amplitude of system (2) at the low-frequency ω of the input signal.

2.2 *Analysis of the vibrational resonance*

In order to verify the theoretical predictions to be obtained from the analysis of Q given by eq. (11a), Q is calculated from the numerical solution of eq. (2). The formula $Q = \sqrt{Q_{\text{s}}^2 + Q_{\text{c}}^2}/f$ is used where [3,5,13]

$$Q_{\text{s}} = \frac{2}{nT}\int_0^{nT} x(t)\sin\omega t\ \text{d}t, \tag{12a}$$

$$Q_{\text{c}} = \frac{2}{nT}\int_0^{nT} x(t)\cos\omega t\ \text{d}t, \tag{12b}$$

with $T = 2\pi/\omega$ and n is big enough, say 500.

The value of a control parameter at which resonance occurs (Q becomes maximum) corresponds to the minimum of the function S given by eq. (11a). The following are the key results of analysis of the theoretical expression of the response amplitude Q.

- For a fixed value of g when ω is varied, resonance occurs when $\omega = \omega_{\rm VR}$ where $\omega_{\rm VR}$ is given by (obtained from $\mathrm{d}S/\mathrm{d}\omega = 0$)

$$\omega_{\rm VR} = \sqrt{\omega_{\rm r}^2 - \frac{d^2}{2}}, \qquad \omega_{\rm r}^2 > \frac{d^2}{2}. \tag{13}$$

- When g is varied the condition for resonance is $\mathrm{d}S/\mathrm{d}g = 4\omega_{\rm r}\omega_{\rm rg}(\omega_{\rm r}^2 - \omega^2) = 0$. Because I_0 is always >0 and increases monotonically with g we have $\omega_{\rm r} \neq 0$ and $\omega_{\rm rg} = \mathrm{d}\omega_{\rm r}/\mathrm{d}g \neq 0$ and hence the resonance condition is $\omega_{\rm r}^2 = \omega^2$, that is, $\beta I_0^2(g/\Omega^2)/I_0(2g/\Omega^2) = \omega^2$. Resonance occurs whenever the resonant frequency $\omega_{\rm r}$ matches with the low-frequency ω of the periodic force.
- Figures 3a and b show the variation of the response amplitude Q and $\omega_{\rm r}^2$ respectively with g for three fixed values of β and $d = 0.5,\ f = 0.1,\ \omega = 1$ and $\Omega = 10$. The theoretical value of Q is in very good agreement with Q obtained from the numerical solution of eq. (2). In figure 3a, for both $\beta = 2$ and 1.5, as g increases from zero the value of Q increases monotonically, it reaches a maximum at $g = g_{\rm VR}$ and then decreases. For $\beta = 2$, the theoretical and numerical values of $g_{\rm VR}$ are 176 and 173 respectively. In figure 3b for both $\beta = 2$ and 1.5 at $g = g_{\rm VR}$ (indicated by solid circles), $\omega_{\rm r}^2 = \omega^2$.
- At $g = 0$, $I_0(\mu) = I_0(2\mu) = 1$ and $\omega_{\rm r}^2(g = 0) = \beta$. As g increases, $I_0(\mu)$ and $I_0(2\mu)$ increase rapidly with $I_0(2\mu)$ growing faster than $I_0(\mu)$ as shown in figure 2a. Consequently, $\omega_{\rm r}^2$ decreases rapidly from the value of β for a while and then decays to zero slowly. The maximum value of $\omega_{\rm r}^2$ is β and this happens at $g = 0$. For $\beta < \omega^2$, $\omega_{\rm r}^2$ is always less than ω^2, that is, $\omega_{\rm r}^2 \neq \omega^2$ for $g > 0$ implying no resonance. This is shown in figure 3a for $\beta = 0.5$ and $\omega = 1$ for which Q decreases continuously with g.
- Resonance is possible only for $\beta > \omega^2$. In this case, as g increases from zero, $\omega_{\rm r}^2$ decreases and becomes ω^2 at only one value. Hence, there is only one resonance.

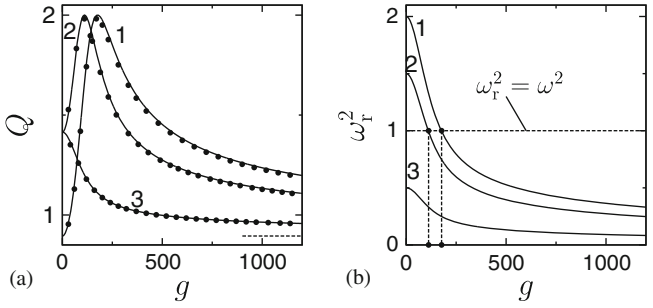

Figure 3. (**a**) Response amplitude Q vs. the control parameter g for the Morse oscillator for three values of β. The values of the parameters are $d = 0.5,\ f = 0.1,\ \omega = 1$ and $\Omega = 10$. The values of β for the curves 1, 2 and 3 are 2, 1.5 and 0.5 respectively. The continuous curve and solid circles represent theoretically and numerically computed values of Q respectively. The horizontal dashed line denotes the limiting value of Q, $Q_{\rm L}(g \to \infty)$. (**b**) Dependence of $\omega_{\rm r}^2$ with g for the three values of β used in figure 3a. The solid circles on the g axis denote the values of g at which resonance occurs.

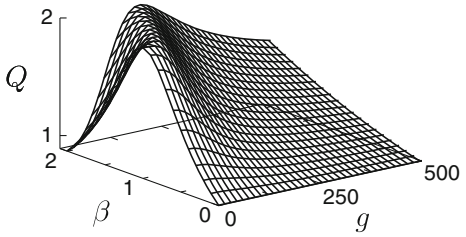

Figure 4. Three-dimensional plot of the theoretically computed response amplitude Q as a function of β and g.

This is shown in figure 3a for $\beta = 1.5$ and 2 with $\omega = 1$. Figure 4 presents the dependence of Q on β and g for $\omega = 1$. Resonance is seen only for $\beta > \omega^2 (= 1)$.

- At resonance $\omega_r^2 = \omega^2$ and hence $Q_{max} = 1/d\omega$ and it depends only on d and ω. The response amplitude at resonance is independent of the parameters β, g and Ω.
- An analytical expression for g_{VR} (at which Q becomes maximum) is difficult to obtain because ω_r^2 is a complicated function of g. However, g_{VR} can be calculated from the resonance curve. It depends on Ω, ω and β and independent of d and f. Q decreases with increase in the value of d. In figure 5 we plot the theoretically predicted g_{VR} and numerically computed g_{VR} vs. the parameter β for a few fixed values of ω. g_{VR} increases with increase in the value of β.
- For very large values of g, $\omega_r^2 \to 0$ and Q approaches the limiting value Q_L given by

$$Q_L(g \to \infty) = \frac{1}{\omega\sqrt{\omega^2 + d^2}}. \tag{14}$$

That is, Q does not decay to zero but approaches the above limiting value (see figure 3a). This limiting value depends only on the parameters ω and d (note that $Q_{max} = 1/d\omega$). The point is that when $\omega_r^2 \to 0$, eq. (9) becomes the damped free particle driven by the periodic force whose solution is

$$Y(t) = Q_L f \cos(\omega t + \Phi), \quad \Phi = \tan^{-1}(d/\omega). \tag{15}$$

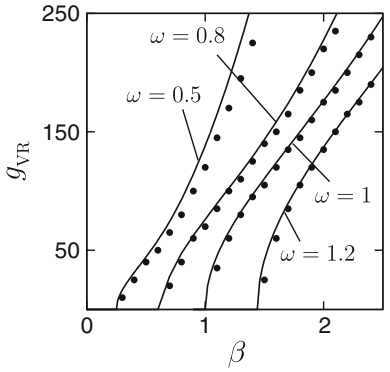

Figure 5. Variation of theoretically predicted (continuous curve) and numerically computed (solid circles) g_{VR} with the parameter β for a few fixed values of the parameter ω. The value of Ω is 10ω.

For the Duffing and quintic oscillators [3,5,11,25] $V(x)$ (as well as the effective potential) $\to \infty$ as $x \to \pm\infty$. In this case the resonant frequency diverges after a few oscillations and thus Q decays to zero for large values of g.

3. Resonance with a square-wave signal

In this section we show that vibrational resonance can be realized in the Morse oscillator when the external signal is a square-wave and the theoretical analysis employed in the previous section for sinusoidal force can be applied to this case also.

In system (2), in place of $F_1 = f\cos\omega t + g\cos\Omega t$, we consider three other forms of external force given by

$$F_2(t) = f\cos\omega t + g\,\mathrm{sgn}(\cos\Omega t), \tag{16}$$

$$F_3(t) = f\,\mathrm{sgn}(\cos\omega t) + g\cos\Omega t, \tag{17}$$

$$F_4(t) = f\,\mathrm{sgn}(\cos\omega t) + g\,\mathrm{sgn}(\cos\Omega t), \tag{18}$$

where $\mathrm{sgn}|u|$ denotes sign of u. In the theoretical analysis we use a Fourier series expansion for the square-wave signal. For the Morse oscillator driven by the periodic force $F_2(t)$ the solution of slow motion is $Y_2 = Q_2 f\cos(\omega t + \phi_2)$ where

$$Q_2 = \frac{1}{\sqrt{(\omega_{\mathrm{r},2}^2 - \omega^2)^2 + d^2\omega^2}}, \tag{19a}$$

where

$$\omega_{\mathrm{r},2}^2 = \frac{\beta U^2(\mu)}{U(2\mu)}, \quad U(\mu) = \frac{1}{2\pi}\int_0^{2\pi} \mathrm{e}^{-\psi_2}\,\mathrm{d}\tau, \tag{19b}$$

$$\psi_2 = \frac{4\mu}{\pi}\sum_{n=0}^{\infty}\frac{(-1)^{n+1}\cos(2n+1)\tau}{(2n+1)^3}. \tag{19c}$$

For the system driven by the force F_3, the solution Y_3 is

$$Y_3 = \frac{4f}{\pi}\sum_{n=0}^{\infty}\frac{(-1)^n}{(2n+1)}\frac{\cos[(2n+1)\omega t + \phi_3]}{[(\omega_{\mathrm{r},3}^2 - (2n+1)^2\omega^2)^2 + (2n+1)^2 d^2\omega^2]^{1/2}}, \tag{20a}$$

where

$$\omega_{\mathrm{r},3}^2 = \frac{\beta I_0^2(\mu)}{I_0(2\mu)}. \tag{20b}$$

The solution Y_3 has frequencies ω and odd integer multiples of it. The response amplitude Q_3 corresponding to the fundamental frequency ω is

$$Q_3 = \frac{4}{\pi}\frac{1}{\sqrt{(\omega_{\mathrm{r},3}^2 - \omega^2)^2 + d^2\omega^2}}. \tag{21}$$

When the biharmonic force is chosen as F_4 given by eq. (18) then the expression for the solution Y_4 is the same as Y_3 except that now $\omega_{\mathrm{r},3}^2$ is replaced by $\omega_{\mathrm{r},4}^2$ where

$$\omega_{\mathrm{r},4}^2 = \frac{\beta U^2(\mu)}{U(2\mu)}. \tag{22}$$

Then

$$Q_4 = \frac{4}{\pi} \frac{1}{\sqrt{(\omega_{\mathrm{r},4}^2 - \omega^2)^2 + d^2\omega^2}} \,. \tag{23}$$

Figure 6 shows both theoretically determined Q and numerically computed Q vs. g with different input signals where $d = 0.5,\ \beta = 2,\ f = 0.1,\ \omega = 1$ and $\Omega = 10$. In this figure, apart from the close agreement of theoretical Q with numerical Q, we notice that $Q_{1,\max} = Q_{2,\max}$, $Q_{3,\max} = Q_{4,\max}$, $Q_{1,\mathrm{L}} = Q_{2,\mathrm{L}}$ (limiting values of Q in the limit of $g \to \infty$) and $Q_{3,\mathrm{L}} = Q_{4,\mathrm{L}}$. These results can be accounted from the theoretical expressions of Q_i. The resonance condition $\omega_{\mathrm{r},i}^2 = \omega^2$, $i = 1,\ 2,\ 3,\ 4$ in the expression of Q_i gives

$$Q_{1,\max} = Q_{2,\max} = \frac{1}{d\omega}, \tag{24a}$$

$$Q_{3,\max} = Q_{4,\max} = \frac{4}{\pi d\omega} = \frac{4}{\pi} Q_{1,\max}, \tag{24b}$$

that is, $Q_{3,\max}$ and $Q_{4,\max}$ are $4/\pi \approx 1.27324$ times of $Q_{1,\max}$. For the parametric values used in our analysis, $Q_{1,\max} = 2$ and hence $Q_{3,\max}$ and $Q_{4,\max}$ are 2.54648 as is the case in figure 6. For sufficiently large values of g, $\omega_{\mathrm{r},i}^2 \approx 0$ and hence

$$Q_{1,\mathrm{L}} = Q_{2,\mathrm{L}} = \frac{1}{\omega\sqrt{\omega^2 + d^2}}, \qquad Q_{3,\mathrm{L}} = Q_{4,\mathrm{L}} = \frac{4}{\pi} Q_{1,\mathrm{L}}. \tag{25}$$

Furthermore, because of $\omega_{\mathrm{r},1}^2 = \omega_{\mathrm{r},3}^2$ and $\omega_{\mathrm{r},2}^2 = \omega_{\mathrm{r},4}^2$ it is found that

$$Q_3 = \frac{4}{\pi} Q_1, \qquad Q_4 = \frac{4}{\pi} Q_2. \tag{26}$$

That is, the response amplitude at frequency ω when the input signal is a square-wave with fundamental frequency being ω is $4/\pi$ times that of the signal $f \cos \omega t$. Numerical results in figure 6 confirms all the above theoretical predictions.

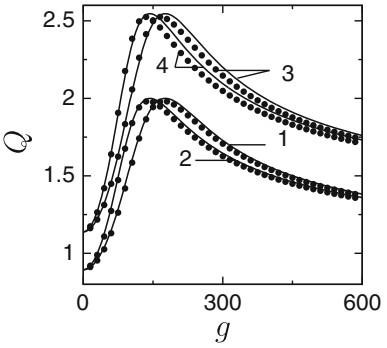

Figure 6. Variation of the response amplitude Q with g for four different types of biharmonic forces. The continuous curves and the solid circles represent theoretically calculated Q and numerically calculated Q respectively. The biharmonic forces corresponding to the curves and solid circles marked as 1, 2, 3 and 4 are $f \cos \omega t + g \cos \Omega t$, F_2, F_3 and F_4 respectively.

Our analysis shows that the form of the low- and high-frequency forces need not be identical. For any arbitrary force containing a component with frequency ω, enhancement of the amplitude of the output signal at frequency ω can be achieved by using another arbitrary force containing a frequency $\Omega \gg \omega$. When the force involved is simple periodic function of t, then the theoretical analysis of vibrational resonance is very much feasible.

4. Quantum mechanical Morse oscillator

In the previous two sections, our analysis was focussed on vibrational resonance in the classical Morse oscillator. In the present section we are concerned with the quantum mechanical Morse oscillator in the presence of biharmonic external field $W(t) = F\cos\omega t + g\cos\Omega t$ with $\Omega \gg \omega$. When a quantum mechanical system is subjected to a time-dependent external field, the system undergoes transition between the energy eigenstates. Therefore, we are interested in knowing the probability of finding the system in an fth state at time t.

The unperturbed Hamiltonian of the system is $H_0 = (p_x^2/2m) + V(x)$ where $V(x)$ is given by eq. (1). The unperturbed system $H_0\phi_n = E_n\phi_n$ is exactly solvable and the eigenfunctions and energy eigenvalues are given by [38–40]

$$\phi_n = N_n z^{\lambda-n-1/2}\,\mathrm{e}^{-z/2}L_n^k(z), \tag{27a}$$

where

$$z = 2\lambda\mathrm{e}^{-x}, \quad \lambda^2 = \frac{m\beta}{\hbar^2}, \quad N_n = \left(\frac{kn!}{(2\lambda-n-1)!}\right)^{1/2}, \tag{27b}$$

$$k = 2\lambda - 2n - 1, \quad L_n^k(z) = \frac{z^{-k}\mathrm{e}^z}{n!}\frac{\mathrm{d}^n}{\mathrm{d}z^n}\mathrm{e}^{-z}z^{n+k} \tag{27c}$$

and

$$E_n = -\frac{\hbar^2}{2m}\left(\lambda - n - \frac{1}{2}\right)^2, \qquad n = 0, 1, \ldots \quad \text{and} \quad n < \lambda - \frac{1}{2}. \tag{28}$$

In eq. (27c), $L_n^k(z)$ are the generalized Laguerre polynomials. The Morse oscillator has a finite number of bound states and the number of bound states can be controlled by the parameter β. Setting the values of $\hbar$ and m as unity for convenience and $\beta = 9$ we obtain

$$E_0 = -3.125, \quad E_1 = -1.125, \quad E_2 = -0.125. \tag{29}$$

There are only three bound states. Figure 7 shows the energy eigenvalues and the eigenfunctions for $\beta = 9$.

In the presence of external field, the Hamiltonian of the system is $H = H_0 + \epsilon H_1$, where $H_1 = xW(t)$. The time-dependent Schrödinger equation for the system is

$$\mathrm{i}\hbar\frac{\partial\psi}{\partial t} = H\psi, \tag{30}$$

where $\psi(x,t)$ is the wave function of the perturbed system. We write

$$\psi(x,t) = \sum_n a_n(t)\phi_n(x)\mathrm{e}^{-\mathrm{i}E_nt/\hbar}. \tag{31}$$

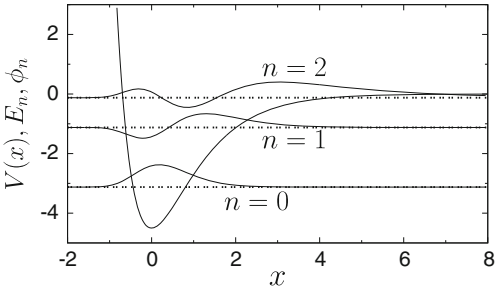

Figure 7. Bound state energy eigenvalues and eigenfunctions of the Morse oscillator for $\beta = 9$. The dashed lines are the energy eigenvalues. The potential $V(x)$ is also shown.

The probability of finding the system in the state n is $P_n(t) = |a_n(t)|^2$, $\sum_n |a_n(t)|^2 = 1$.

To determine $a_n(t)$ we apply the standard time-dependent perturbation theory [41]. Suppose the external field is switched-on at $t = 0$ and switched-off at $t = T$, that is, the external field is applied during a finite time interval T. Assume that the system is initially in a state i with the eigenfunction ϕ_i. Then at $t = 0$ the probability of finding the system in the state i is 1 and the probability of finding the system in the other states is 0: $a_n(0) = \delta_{ni}$. Due to the applied field the system can make a transition from the state i to an another state after the time T. Once the perturbation is switched-off, the system settles down to a stationary state and this final state is denoted as f.

To determine $a_n(t)$ we substitute eq. (31), $a_f = a_f^{(0)} + \epsilon a_f^{(1)} + \cdots$ and equate the terms containing various powers of ϵ to 0. Up to first order in ϵ, after some algebra, we obtain $a_f^{(0)} = \delta_{fi}$ and

$$a_f^{(1)}(T) = \frac{C_{fi}}{2\hbar} s, \tag{32a}$$

where

$$s = F(r_{1+} + r_{1-}) + g(r_{2+} + r_{2-}), \tag{32b}$$

$$r_{1\pm} = \frac{1 - \mathrm{e}^{\mathrm{i}(\omega_{fi} \pm \omega)T}}{\omega_{fi} \pm \omega}, \qquad r_{2\pm} = \frac{1 - \mathrm{e}^{\mathrm{i}(\omega_{fi} \pm \Omega)T}}{\omega_{fi} \pm \Omega}, \tag{32c}$$

$$\omega_{fi} = \frac{(E_f - E_i)}{\hbar}, \qquad C_{fi} = \int_{-\infty}^{\infty} \phi_f^* x \phi_i \, \mathrm{d}x. \tag{32d}$$

The transition probability for ith state to fth state is given by $P_{fi}(T) = |\delta_{fi} + \epsilon a_f^{(1)}(T)|^2$. In $a_f^{(1)}(T)$ the term s alone depends on the parameters F, ω, g and Ω of the external field and T. Therefore, we study the variation of the quantity $|s|^2$ with the parameters of the external field.

We fix $\beta = 9$, $F = 0.05$, $T = \pi$ and assume that the system is initially in the ground state ($i = 0$). Figure 8 shows the variation of $\log|s|^2$ with ω for $g = 0$. The first-order correction to transition probability displays a sequence of resonance peaks with

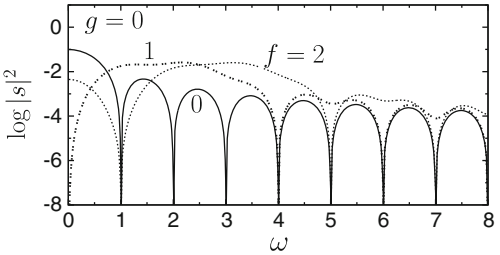

Figure 8. $\log|s|^2$ vs. ω for the states $f = 0$, 1 and 2 for $\beta = 9$, $F = 0.05$, $g = 0$, $T = \pi$ and $i = 0$.

decreasing amplitude. The following results are evident from eqs (32b) and (32c) and figure 8. The quantity s consists of only r_{1+} and r_{1-}. We have $\omega_{00} = 0$, $\omega_{10} = 2$ and $\omega_{20} = 3$. Consequently, for the states $f = 0$, 1 and 2 the quantity r_{1+} can be neglected when $\omega \approx 0$, 2 and 3 respectively because the denominator in r_{1-} is ≈ 0. Thus, the first-order transition probability for the states $f = 0$, 1 and 2 becomes maximum at $\omega = 0$, 2 and 3 respectively. For $\omega \approx 0$ the values of $|s|^2$ for $f = 0$, 1 and 2 are $\approx 4F^2\pi^2$, 0 and $16F^2/9$ respectively. The first-order transition probability for the state $f = 1$ is ≈ 0. For the $f = 0$ state $|s|^2 = 0$ when $\omega = 1, 2, \ldots$ and it becomes maximum when $\omega = n + \frac{1}{2}$, $n = 1, 2, \ldots$. When $f = 1$ at $\omega = 4, 6, \ldots$ the numerators in both r_{1+} and r_{1-} become zero and thus the quantity $|s|^2$ is minimum. For $f = 2$, at odd integer values of ω except at $\omega = 3$, $r_{1\pm} = 0$ and hence $|s|^2$ becomes minimum.

Next, we include the high-frequency field and vary its amplitude g and the frequency Ω. Figure 9 presents the results for a few fixed values of ω with $\Omega = 5\omega$. When $\omega = 1$, in eq. (32b), $r_{1+} + r_{1-} = 0$ and $r_{2+} + r_{2-} = 0$ for $f = 0$ and 2 and hence the increase of g has no effect on $|s|^2$. For the $f = 1$ state we find $s = (8/3)F - (8/21)g$. As g increases $|s|^2$ decreases from $(8/3)F$, becomes 0 at $g = 7F(= 0.35)$ and then increases with further increase in g as shown in figure 9a. The first-order transition probability of the state $f = 1$ exhibits antiresonance at $g = 0.35$. Antiresonance can be realizable for other states also for appropriate choices of ω. For example, in figures 9b and c corresponding to $\omega = 1.7$ and 2 respectively we can clearly notice antiresonance for $f = 0$ and 2 states. In figure 9d where $\omega = 3.5$ the quantity $|s|^2$ increases monotonically with the control parameter g for all the three states.

As r_{2+} and r_{2-} (given by eq. (32c)) contain terms which are sinusoidal functions of Ω, the first-order transition probability can exhibit a sequence of resonance peaks when Ω is varied for fixed values of other parameters. This is shown in figure 10 for four sets of values of ω and g. In all the cases Ω is varied from 5ω. In figures 10a–c, $|s|^2 = 0$ at the starting value of Ω for the $f = 0$ state. $|s|^2 \neq 0$ for wide ranges of values of Ω. Transition probability of all the states show a sequence of resonance peaks. In figure 10d $|s|^2$ of $f = 0$ state is close to its values of the other two states. However, as Ω increases $|s|^2$ of the $f = 1$ and $f = 2$ states oscillate but $\neq 0$. In contrast to this, $|s|^2$ of the $f = 0$ state becomes 0 at certain values of Ω.

It is noteworthy to compare the effect of high-frequency external force in the classical and quantum mechanical Morse oscillators. A classical nonlinear system can exhibit a

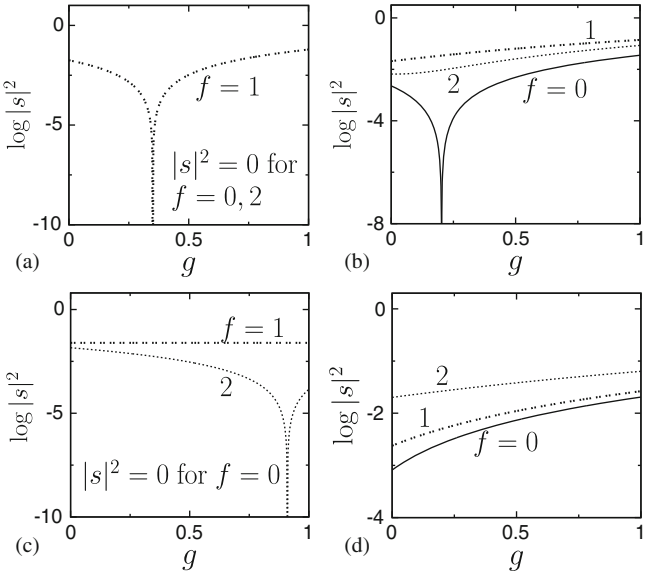

Figure 9. Variation of $|s|^2$ (in log scale) with the amplitude g of the high-frequency external field for (**a**) $\omega = 1$, (**b**) $\omega = 1.7$, (**c**) $\omega = 2$, (**d**) $\omega = 3.5$ of the low-frequency external field. The value of Ω is fixed as 5ω.

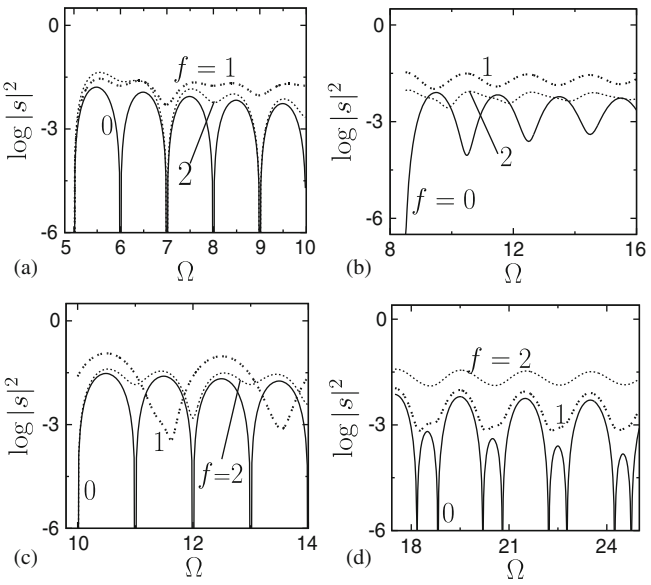

Figure 10. $\log|s|^2$ vs. Ω (the frequency of the high-frequency external field) for (**a**) $\omega = 1$, $g = 0.35$, (**b**) $\omega = 1.7$, $g = 0.2$, (**c**) $\omega = 2$, $g = 0.91$ and (**d**) $\omega = 3.5$ $g = 0.5$.

variety of dynamics when a control parameter is varied. However, in the Morse oscillator for the choice $|f| \ll 1$ and $\Omega \gg \omega$ when the amplitude g of the high-frequency force is varied the system is found to show only periodic motion with period $T = 2\pi/\omega$. The response amplitude of the motion exhibits a single resonance when the control parameter g or ω or Ω is varied. Resonance occurs whenever the resonant frequency ω_r (eq. (9b)) matches with the frequency ω. In the case of the quantum mechanical Morse oscillator, we have considered the simple case of switching-on the external field at $t = 0$ and switching-off the external field at $t = T$. In the absence of high-frequency field, the first-order transition probability P_{fi} shows a sequence of resonances with decreasing amplitude when the parameter ω is increased. The dominant resonance occurs at $\omega = \omega_{fi}$. Resonance is not observed when the amplitude g of the high-frequency field is varied. However, antiresonance of P_{fi} takes place for certain values of ω. Multiple resonance of P_{fi} occurs when the frequency Ω of the high-frequency field is varied.

5. Conclusion

The investigation on high-frequency periodic force-induced resonance at the low-frequency component of the output of a single oscillator was reported here. Using a perturbation theory, an analytical expression for the response amplitude is obtained. Interestingly, from the analytical expression of Q it was possible to derive various features of the vibrational resonance and its mechanisms. The occurrence of the resonance depends on the parameter β and ω while the values of the response amplitude at resonance and for large values of g depend only on the damping coefficient d and the low-frequency ω. In the system the limiting values of Q is nonzero because for sufficiently large values of g, $\omega_r^2 \approx 0$. From the analytical expression of Q given by eq. (11a) it was noted that Q becomes a nonzero constant if $\omega_r^2 \approx$ a constant. The theory used in this analysis can be applied to different forms of input signal other than $\cos\omega t$ and $\sin\omega t$. Its applicability for the case of square-wave form was demonstrated here. All the theoretical results are well supported by the numerical simulation. The quantum version of the Morse oscillator in the presence of biharmonic external field was also considered. Interestingly, a high-frequency external field is found to induce resonance and antiresonance on the transition probability for the transition from an ith state to an fth state. If the transition probability P_{fi} of a state is weak in the presence of a harmonic external field with a particular frequency ω, then it can be enhanced by another external field of relatively high frequency. The dominance of a state can be changed by the high-frequency external field. That is, P_{fi} can be controlled by a second harmonic external field.

Acknowledgements

KA acknowledges the support from University Grants Commission (UGC), India in the form of UGC-Rajiv Gandhi National Fellowship. Financial support from the Spanish Ministry of Science and Innovation under Project No. FIS2009-09898 is acknowledged by MAFS.

References

[1] L Gammaitoni, P Hänggi, P Jung and F Marchesoni, *Rev. Mod. Phys.* **70**, 223 (1998)
[2] M D McDonnell, N G Stocks, C E M Pearce and D Abbott, *Stochastic resonance* (Cambridge University Press, Cambridge, 2008)
[3] P S Landa and P V E McClintock, *J. Phys. A: Math. Gen.* **33**, L433 (2000)
[4] M Gittermann, *J. Phys. A: Math. Gen.* **34**, L355 (2001)
[5] I I Blechman and P S Landa, *Int. J. Nonlin. Mech.* **39**, 421 (2004)
[6] V In, A Kho, J D Neff, A Palacios, P Loghini and B K Meadows, *Phys. Rev. Lett.* **91**, 244101 (2003)
[7] V In, A R Bulsara, A Palacios, P Loghini and A Kho, *Phys. Rev. E* **72**, 045104(R) (2005)
[8] B J Breen, A B Doud, J R Grimm, A H Tanasse, S J Janasse, J F Lindner and K J Maxted, *Phys. Rev. E* **83**, 037601 (2011)
[9] E Ippen, J Lindner and W L Ditto, *J. Stat. Phys.* **70**, 437 (1993)
[10] S Zambrano, J M Casado and M A F Sanjuan, *Phys. Lett. A* **366**, 428 (2007)
[11] S Jeyakumari, V Chinnathambi, S Rajasekar and M A F Sanjuan, *Phys. Rev. E* **80**, 046608 (2009)
[12] S Rajasekar, K Abirami and M A F Sanjuan, *Chaos* **21**, 033106 (2011)
[13] E Ullner, A Zaikin, J Garcia-Ojalvo, R Bascones and J Kurths, *Phys. Lett. A* **312**, 348 (2003)
[14] H Yu, J Wang, C Liu, B Deng and X Wei, *Chaos* **21**, 043101 (2011)
[15] V M Gandhimathi, S Rajasekar and J Kurths, *Phys. Lett. A* **360**, 279 (2006)
[16] B Deng, J Wang and X Wei, *Chaos* **19**, 013117 (2009)
[17] B Deng, J Wang, X Wei, K M Tsang and W L Chan, *Chaos* **19**, 013113 (2010)
[18] V N Chizhevsky, E Smeu and G Giacomelli, *Phys. Rev. Lett.* **91**, 220602 (2003)
[19] V N Chizhevsky and G Giacomelli, *Phys. Rev. E* **70**, 062101 (2004)
[20] V N Chizhevsky and G Giacomelli, *Phys. Rev. E* **73**, 022103 (2006)
[21] J P Baltanas, L Lopez, I I Blechman, P S Landa, A Zaikin, J Kurths and M A F Sanjuan, *Phys. Rev. E* **67**, 066119 (2003)
[22] C Yao, Y Liu and M Zhan, *Phys. Rev. E* **83**, 061122 (2011)
[23] C Yao and M Zhan, *Phys. Rev. E* **81**, 061129 (2010)
[24] S Rajasekar, J Used, A Wagemakers and M A F Sanjuan, *Commun. Nonlin. Sci. Numer. Simulat.* **17**, 3435 (2012)
[25] S Jeyakumari, V Chinnathambi, S Rajasekar and M A F Sanjuan, *Chaos* **21**, 275 (2011)
[26] J H Yang and X B Liu, *J. Phys. A: Math. Theor.* **43**, 122001 (2010)
[27] J H Yang and X B Liu, *Chaos* **20**, 033124 (2010)
[28] C Jeevarathinam, S Rajasekar and M A F Sanjuan, *Phys. Rev. E* **83**, 066205 (2011)
[29] J H Yang and X B Liu, *Phys. Scr.* **83**, 065008 (2011)
[30] A Ichiki, Y Tadokoro and M I Dykman, *Phys. Rev. E* **85**, 031107 (2012)
[31] J R Ackerhalt and P W Milonni, *Phys. Rev. A* **34**, 1211 (1986)
[32] M E Goggin and P W Milonni, *Phys. Rev. A* **37**, 796 (1988)
[33] D Beigie and S Wiggins, *Phys. Rev. A* **45**, 4803 (1992)
[34] A Memboeuf and S Aubry, *Physica D* **207**, 1 (2005)
[35] W Knob and W Lauterborn, *J. Chem. Phys.* **93**, 3950 (1990)
[36] Z Jing, J Deng and J Yang, *Chaos, Solitons and Fractals* **35**, 486 (2008)
[37] K T Tang, *Mathematical methods for engineers and scientists: Fourier analysis, partial differential equations and variational models* (Springer, Berlin, 2007) p. 191
[38] A Frank, R Lemus, M Carvajal, C Jung and E Ziemniak, *Chem. Phys. Lett.* **308**, 91 (1999)
[39] R Lemus and A Frank, *Chem. Phys. Lett.* **349**, 471 (2001)
[40] R Lemus, *J. Mol. Spectrosc.* **225**, 73 (2004)
[41] L I Schiff, *Quantum mechanics* (McGraw-Hill, New York, 1968)